QED background against atomic neutrino process with initial spatial phase

Tanaka, Minoru
Department of Physics, Graduate School of Science, Osaka University

Tsumura, Koji
Department of Physics, Kyushu University

Sasao, Noboru
Research Institute for Interdisciplinary Science, Okayama University

Uetake, Satoshi
Research Institute for Interdisciplinary Science, Okayama University

他

https://hdl.handle.net/2324/4822544

QED background against atomic neutrino process with initial spatial phase

Minoru Tanaka [*][1], Koji Tsumura[2], Noboru Sasao[3], Satoshi Uetake[3], and Motohiko Yoshimura[3]

[1]*Department of Physics, Graduate School of Science, Osaka University, Toyonaka, Osaka 560-0043, Japan*
[2]*Department of Physics, Kyushu University, 744 Motooka, Nishi-ku, Fukuoka, 819-0395, Japan*
[3]*Research Institute for Interdisciplinary Science, Okayama University, Tsushima-naka 3-1-1, Kita-ku, Okayama 700-8530, Japan*

December 6, 2019

Abstract

Atomic deexcitation emitting a neutrino pair and a photon is expected to provide a novel method of neutrino physics if it is enhanced by quantum coherence in a macroscopic target. However, the same enhancement mechanism may also lead to a serious problem of enhanced QED background process. We show that the QED background can be suppressed enough in the photonic crystal waveguide by using the spatial phase that is imprinted in the process of initial coherence generation in the target at excitation.

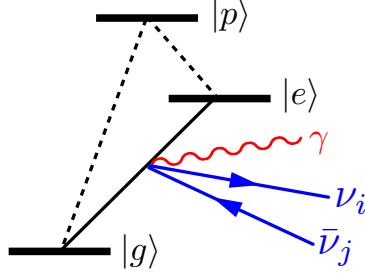[*]Email: tanaka@phys.sci.osaka-u.ac.jp

Figure 1: RENP scheme. A virtual intermediate state $|p\rangle$ is shown as well as an excited initial state $|e\rangle$ and the final ground state $|g\rangle$

.

1 Introduction

Neutrino pair emission in atomic transitions, which can produce nonrelativistic neutrinos, is conceived to further clarify neutrino properties. Important questions to be addressed include the absolute values of neutrino masses and the discrimination of "Dirac or Majorana" nature. Radiative emission of neutrino pair (RENP), $|e\rangle \to |g\rangle + \gamma + \nu_i + \bar{\nu}_j$, has been considered as a candidate of such atomic neutrino processes in Refs. [1, 2], where $|e\rangle$ and $|g\rangle$ are a metastable excited state and the ground state of an atom respectively, and i and j specify neutrino mass eigenstates. Three flavor scheme is assumed in the present work, hence $i, j = 1, 2, 3$. The second order perturbation of QED and the weak four-fermion interaction via a virtual intermediate state $|p\rangle$ leads to RENP process as depicted in Fig. 1.

RENP rate is quantitatively predictable in the standard model of particle physics augmented by a mechanism of generating finite neutrino masses and mixings and turns out to be strongly suppressed for an isolated atom owing to its extremely low energy scale ($\sim$ eV). To overcome this small rate, an enhancement mechanism that makes use of quantum coherence in a macroscopic target [3], called macrocoherence, is employed in the proposed experimental scheme [1, 2].

As a proof-of-concept of the macrocoherent amplification, the QED two-photon process in which a photon substitutes for the neutrino pair of RENP, $|e\rangle \to |g\rangle + \gamma + \gamma$, has been studied both theoretically [4] and experimentally [5, 6, 7, 8]. In a series of experiments, the rate enhancement of $O(10^{18})$ was observed.

In addition to the remarkable rate amplification, the effective momentum conservation, $\boldsymbol{p}_{eg} = \boldsymbol{p}_\gamma + \boldsymbol{p}_i + \boldsymbol{p}_j$, is the prominent feature of the macrocoherence, where $\boldsymbol{p}_{\gamma,i,j}$ are momenta of the emitted particles and $\boldsymbol{p}_{eg}$ gives the initial spatial phase (ISP) $e^{i\boldsymbol{p}_{eg}\cdot\boldsymbol{x}}$ in the macroscopic target created at excitation. We shall explain more on this. We note that the momentum conservation, or atomic recoil, may be neglected to a good approximation in ordinary atomic radiation processes because of very small atomic recoil. The macrocoherent momentum conservation holds irrespective of very small atomic recoil. It corresponds to the phase-matching condition in the quantum electronics.

We can regard $\boldsymbol{p}_{eg}$ of the ISP as the momentum of the parent particle. Combined with the energy conservation, the RENP process follows the same kinematics as in the three-
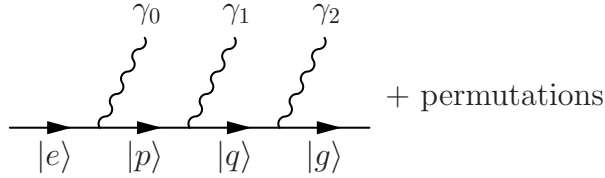
Figure 2: Feynman diagram of McQ3. Possible permutations of the photons are not explicitly shown.

body decay of a particle of four-momentum $(E_{eg}, \boldsymbol{p}_{eg})$, where E_{eg} is the level splitting between $|e\rangle$ and $|g\rangle$. The four-momentum conservation results in the six thresholds in the photon energy for possible neutrino pairs of (i, j). Hence, information on the neutrino masses can be obtained from the photon spectrum in RENP. The threshold location in the RENP spectrum can be searched by a frequency scan of the trigger laser.

RENP process with a nonvanishing $\boldsymbol{p}_{eg}$, called boosted RENP, is studied in detail in Ref. [9]. We can arrange the effective mass of the initial state, $\sqrt{E_{eg}^2 - \boldsymbol{p}_{eg}^2}$, at will by varying $\boldsymbol{p}_{eg}$, so that the effective range of neutrino masses in the RENP spectrum is varied. In this work, we make use of $\boldsymbol{p}_{eg}$ to control the QED background of RENP.

The macrocoherent amplification also applies to QED processes of multiphotons and leads to macrocoherent QED processes of n photons (McQn) [10]. The most dangerous background is the three-photon process, McQ3, $|e\rangle \rightarrow |g\rangle + \gamma_0 + \gamma_1 + \gamma_2$, where γ_0 is the trigger photon and $\gamma_{1,2}$ are dynamical photons. We present the Feynman diagram of McQ3 in Fig. 2. The neutrino pair in RENP is replaced by a pair of extra photons $(\gamma_1 + \gamma_2)$ and thus their kinematics are similar. The whole range of the invariant mass of the RENP neutrino pair is covered by that of the photon pair in McQ3. It is shown that the rate of McQ3 is $O(10^{20})$ Hz, while the amplified RENP rate is order of mHz for a xenon transition [10].

We examined the possibility to suppress McQ3 using the Bragg fiber [11], a kind of hollow-core photonic crystal fibers [12] that exhibit photonic band structures due to the periodicity of refractive index [13]. Loading up the hollow core with the RENP target atoms, the McQ3 process becomes forbidden if one of extra photons in McQ3 is emitted in the band gap of an ideal fiber. RENP neutrinos are not affected by the fiber practically. It has turned out that the Bragg fiber of the index contrast realized in the literature [14] does not have a sufficiently wide band gap to cover the whole phase space of extra photons in McQ3.

We assumed $\boldsymbol{p}_{eg} = 0$ (no boost) in our previous work [13]. In the present work, we study the effect of nonvanishing $\boldsymbol{p}_{eg}$ in McQ3 (boosted McQ3). In particular, we present a method to suppress McQ3 with the Bragg fiber of realistic index contrast by locking the boost factor $\boldsymbol{p}_{eg}$ to the wave vector of the trigger photon (boost-trigger lock, BTL).

The rest of the paper is organized as follows. We briefly review the mechanism of macrocoherent amplification in Sec. 2. The kinematics and rate of the boosted McQ3 in the free space are given in Sec. 3. Section 4 describes the boosted McQ3 in the photonic crystal waveguide as well as the feature of the Bragg fiber. In Sec. 5, we introduce the BTL scheme and present the numerical result of the rate suppression of the boosted

McQ3 in the Bragg fiber. The RENP spectrum in the BTL scheme is also shown in Sec. 5. Section 6 is devoted to our conclusion.

2 Macrocoherent amplification mechanism

Each atom in the macroscopic target of the RENP and its QED background processes may be regarded as the two-level quantum system of the ground state $|g\rangle$ and the excited state $|e\rangle$. The deexcitation process emitting plural particles is described by the operator $A := \sum_a e^{-i \sum_i \boldsymbol{p}_i \cdot \boldsymbol{x}_a} |g\rangle_a {}_a\langle e|$, where $\boldsymbol{x}_a$ is the position of the ath atom in the target and i denotes the emitted particles. We have explicitly shown the phase factor that represents the plane waves of the emitted particles and left out coupling constants and other factors irrelevant in the following discussion in this section.

The deexcitation rate of the initial state $|\Psi\rangle$ is proportional to the squared wave function of the final state, $|A|\Psi\rangle|^2 = \langle\Psi|A^\dagger A|\Psi\rangle = \mathrm{tr} A\hat{\rho} A^\dagger$, where the density operator, $\hat{\rho} := \Pi_a \hat{\rho}_a$, is introduced. It is straightforward to obtain

$$\mathrm{tr} A\hat{\rho} A^\dagger = \sum_{a \neq a'} e^{i \sum_i \boldsymbol{p}_i \cdot (\boldsymbol{x}_{a'} - \boldsymbol{x}_a)} \langle e|\hat{\rho}_a|g\rangle \langle g|\hat{\rho}_{a'}|e\rangle + \sum_a \langle e|\hat{\rho}_a|e\rangle \,, \tag{1}$$

where the subscripts of the state vectors are omitted. The first sum is a double sum and represents the coherent contribution, while the second is single and incoherent. We neglect the latter provided that $|\langle e|\hat{\rho}_a|g\rangle|$ is sizable. The coherence of the target is quantified by $|\langle e|\hat{\rho}_a|g\rangle|$.

Since a metastable state is favored as the upper state $|e\rangle$, we assume that the ordinary electric dipole transition between $|g\rangle$ and $|e\rangle$ is forbidden. It turns out that the two-photon absorption process, $|g\rangle + \gamma + \gamma \to |e\rangle$, is appropriate to prepare the initial state of the RENP with nonvanishing $\langle e|\hat{\rho}_a|g\rangle$. We note that this scheme of coherence generation has already been realized for para-hydrogen [8]. As is described in Ref. [9], the absorption of two photons of four-momenta $(\omega_1, \boldsymbol{k}_1)$ and $(\omega_2, \boldsymbol{k}_2)$ with $\omega_1 + \omega_2 = E_{eg}$ imprints the ISP as $\langle e|\hat{\rho}_a|g\rangle = e^{i\boldsymbol{p}_{eg}\cdot\boldsymbol{x}_a}\rho_{a,eg}$, where $\boldsymbol{p}_{eg} = \boldsymbol{k}_1 + \boldsymbol{k}_2$. In the slowly varying envelope approximation, in which the dependence of $\rho_{a,eg}$ on a is neglected in the leading order, we obtain

$$\mathrm{tr} A\hat{\rho} A^\dagger \simeq |\rho_{eg}|^2 \sum_a e^{i(\boldsymbol{p}_{eg} - \sum_i \boldsymbol{p}_i)\cdot\boldsymbol{x}_a} \sum_{a'} e^{-i(\boldsymbol{p}_{eg} - \sum_i \boldsymbol{p}_i)\cdot\boldsymbol{x}_{a'}} \,. \tag{2}$$

Taking the limit of large number of atoms N and large volume V with the number density $n := N/V$ fixed, we find that the macrocoherently amplified rate is proportional to

$$\mathrm{tr} A\hat{\rho} A^\dagger \simeq |\rho_{eg}|^2 \frac{N^2}{V}(2\pi)^3\delta^3(\boldsymbol{p}_{eg} - \sum_i \boldsymbol{p}_i)\,. \tag{3}$$

The delta function in Eq. (3) combined with the one of the energy conservation, which is not explicitly shown, implies the energy-momentum conservation including the ISP in the macrocoherent processes.

4

3 Boosted McQ3 in the free space

3.1 Kinematics

We consider the McQ3 process with the ISP, $|e\rangle \to |g\rangle + \gamma_0(p_0) + \gamma_1(p_1) + \gamma_2(p_2)$, where the four-momenta of the photons are denoted by p_i ($i = 0, 1, 2$) and γ_0 is the trigger photon. The four-momentum conservation owing to the macrocoherence is expressed as

$$P^\mu = p_0^\mu + p_1^\mu + p_2^\mu \,, \tag{4}$$

where $P^\mu = (E_{eg}, \boldsymbol{p}_{eg})$ and $p_i^\mu = (E_i, \boldsymbol{p}_i)$. The two-photon absorption process of asymmetric antiparallel laser irradiation is supposed to provide $\boldsymbol{p}_{eg}$ so that $P^2 > 0$. We note that, in the relativistic three-body decay kinematics of Eq. (4), the invariant mass of the initial state must be positive for the RENP process with a massive neutrino to take place [9].

It is convenient to introduce the four-momentum of the $\gamma_1\gamma_2$ system,

$$q^\mu := p_1^\mu + p_2^\mu = P^\mu - p_0^\mu \,, \tag{5}$$

where $q^2 > 0$ is also required for the RENP with the neutrino pair including at least one massive neutrino. The temporal and spatial components are explicitly given by

$$(q^0, \boldsymbol{q}) = (E_{eg} - E_0, \boldsymbol{p}_{eg} - \boldsymbol{p}_0) \,, \ q^0 > 0 \,. \tag{6}$$

We obtain the following relation of the photon energy $E_{1,2}$ and the angle $\theta_{1,2}$ between $\boldsymbol{q}$ and the momentum of the each emitted photon by solving $(q - p_{1,2})^2 = 0$,

$$\cos\theta_i = \frac{q^0}{|\boldsymbol{q}|} - \frac{q^2}{2|\boldsymbol{q}|E_i} \,, \ i = 1, 2 \,, \tag{7}$$

or equivalently

$$E_i = \frac{q^2}{2(q^0 - |\boldsymbol{q}|\cos\theta_i)} \,, \ i = 1, 2 \,. \tag{8}$$

The range of E_i is determined by $|\cos\theta_i| \le 1$,

$$E_{i,\max} = \frac{1}{2}(q^0 + |\boldsymbol{q}|) = \frac{1}{2}(E_{eg} - E_0 + |\boldsymbol{p}_{eg} - \boldsymbol{p}_0|) \,, \tag{9}$$

$$E_{i,\min} = \frac{1}{2}(q^0 - |\boldsymbol{q}|) = \frac{1}{2}(E_{eg} - E_0 - |\boldsymbol{p}_{eg} - \boldsymbol{p}_0|) \,. \tag{10}$$

3.2 Free-space rate

The differential spectral rate of McQ3 with a boost $\boldsymbol{p}_{eg}$ in the free space is expressed as

$$\frac{d\Gamma_{\mathrm{FS}}}{dE_1} = \frac{\Gamma_0}{|\boldsymbol{q}|} |D|^2 E_1^2 E_2^2 \,, \tag{11}$$
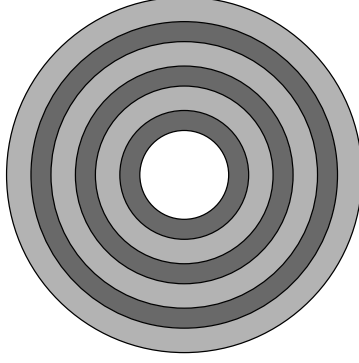
Figure 3: Cross section of the Bragg fiber. The dark (light) gray layers have refractive index n_1 (n_2) and thickness a_1 (a_2).

where $E_2 = E_{eg} - E_0 - E_1$. The energy denominator factor D including all possible permutations in Fig. 2 is defined by

$$
\begin{aligned}
D := \ & \frac{1}{E_{pe} + E_0} \left(\frac{1}{E_{qg} - E_1} + \frac{1}{E_{qe} + E_0 + E_1} \right) \\
& + \frac{1}{E_{pe} + E_1} \left(\frac{1}{E_{qg} - E_0} + \frac{1}{E_{qe} + E_0 + E_1} \right) \\
& + \frac{1}{E_{pg} - E_0 - E_1} \left(\frac{1}{E_{qg} - E_0} + \frac{1}{E_{qg} - E_1} \right) ,
\end{aligned}
\tag{12}
$$

where $E_{pe} := E_p - E_e$ with $E_{p(e)}$ the energy of $|p(e)\rangle$ and similar for the other combinations of states. The overall rate Γ_0 is given by

$$
\Gamma_0 = \frac{3}{2} \pi^2 n^2 V \frac{\gamma_{gq} \gamma_{qp} \gamma_{pe}}{|E_{qg}|^3 |E_{pq}|^3 |E_{ep}|^3} |\mathcal{E}_{\mathrm{trig}}|^2 ,
\tag{13}
$$

where $\mathcal{E}_{\mathrm{trig}}$ denotes the average of the trigger electric field in the target, γ_{gq} is the A coefficient of the transition between $|g\rangle$ and $|q\rangle$ and so on. Equation (11) reproduces the McQ3 rate with no boot (no ISP) in Ref. [10] taking $|\boldsymbol{q}| = E_0$.

4 Boosted McQ3 in the photonic crystal waveguide

It is desired to suppress the boosted McQ3 background by 20 orders or more for observing the RENP process. We have examined the background suppression mechanism by the photonic band gap in the photonic crystal waveguide in the case of no boost [10, 13]. In this section, we apply the same suppression mechanism to the boosted McQ3.

4.1 Bragg fiber and its band structure

We consider the Bragg fiber as an example of photonic crystal waveguides. The cross section of the Bragg fiber is illustrated in Fig. 3. It consists of the hollow core of radius
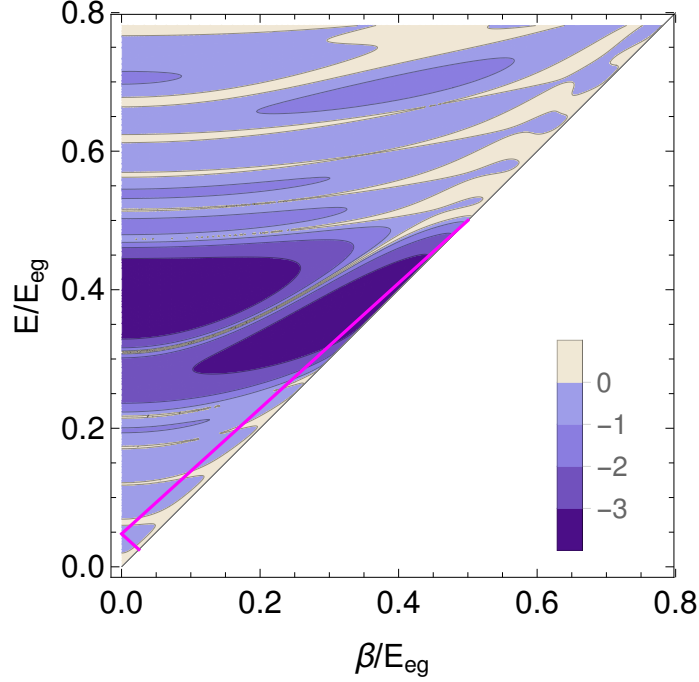
Figure 4: Purcell factor of the Bragg fiber of $(n_1, n_2) = (4.6, 1.6)$. The scale is decimal logarithmic. The solid magenta line indicates the McQ3 physical line.

r_c and the dielectric cladding of N_p layer pairs of alternating refractive indices, n_1 and n_2. The n_1 and n_2 layer thicknesses are a_1 and a_2 respectively.

The emission rate in a cavity like the core of the Bragg fiber is described by the Purcell factor [15], $F_P(E, \beta)$, which is a function of the energy E of photon and the propagation constant β. The latter is the projection of the wave vector onto the propagation (fiber) axis. We introduce

$$\beta_i := E_i |\cos \theta_i|, \ i = 1, 2 \tag{14}$$

for the emitted photons in McQ3, so that β_i is non-negative. This is because of the symmetry of the Bragg fiber under the flip of its axis direction, namely $F_P(E, \beta) = F_P(E, -\beta)$.

The Purcell factor is defined as the ratio of the emission power in the cavity to that in the free space. In the quantum theory of radiation, it is interpreted as the ratio of the state numbers of photon in the cavity and the free space. The calculation of the Purcell factor of the Bragg fiber is described in Ref. [13] in detail.

Figure 4 illustrates the Purcell factor of the Bragg fiber that is designed to suppress the McQ3 with no boost. The relevant fiber parameters are $(n_1, n_2) = (4.6, 1.6)$, $a_2/a_1 = \sqrt{n_1^2 - 1}/\sqrt{n_2^2 - 1} \simeq 3.6$, $r_c/(a_1 + a_2) = 2$ and $N_p = 5$. Darker regions represent stronger suppressions by smaller Purcell factors. The photonic band gap is clearly seen around $E/E_{eg} \sim 0.4$. The solid magenta line represents the physical line on which the McQ3 photons locate in the case of no boost and $E_0 = 0.95 E_{eg}/2$. The expression of the

physical line is easily obtained from Eqs. (7) and (14), and the same for the two emitted photons. In Fig. 4, the period of the cladding (in other words, the lattice spacing of the photonic crystal that specifies the overall scale), $a_1 + a_2$, is chosen to satisfy $E_{eg}(a_1 + a_2) = 0.64$ in order to realize the maximal suppression of the McQ3 with no boost and $E_0 = 0.95 E_{eg}/2$ for the given set of the other fiber parameters.

4.2 Rate in the photonic crystal waveguide

We consider the McQ3 process with a boost in a photonic crystal waveguide like the Bragg fiber. The directions of the boost momentum $\boldsymbol{p}_{eg}$ and the trigger photon momentum $\boldsymbol{p}_0$ are taken to be the same as the direction of the propagation in the waveguide. The rate is written in terms of the free-space one in Eq. (11) and the Purcell factors $F_P(E, \beta)$ as

$$\frac{d\Gamma_{\mathrm{WG}}}{dE_1} = \frac{d\Gamma_{\mathrm{FS}}}{dE_1} F_0 F_1 F_2 \,, \tag{15}$$

where $F_i = F_P(E_i, \beta_i)$ $(i = 0, 1, 2)$, the propagation constant β_0 is given by $\beta_0 = E_0$ and $\beta_{1,2}$ are defined in Eq. (14).

As in the case of no boost [13], the relative improvement of background suppression in the waveguide is quantified by

$$r_{\mathrm{WG/FS}} := \frac{1}{\Gamma_{\mathrm{FS}}(\boldsymbol{p}_{eg}, E_0)} \int \frac{d\Gamma_{\mathrm{FS}}}{dE_1} F_1 F_2 dE_1 \,. \tag{16}$$

We note that the Purcell factor of the trigger F_0 disappears because it is common for the signal (RENP) and the background (McQ3). In order to obtain a sufficient suppression, it is required that at least one of the emitted photons γ_1 and γ_2 is in the band gap of the photonic crystal so that $F_1 F_2$ is tiny in the whole phase space.

5 Method of boost-trigger lock (BTL)

5.1 Problem in the case of no boost

It is shown in our previous work [13], the band gap of the Bragg fiber of $(n_1, n_2) = (4.6, 1.6)$, which is fabricated in the laboratory [14], is not wide enough to suppress the McQ3 rate in the case of no boost. This is due to the rather wide photon spectrum, $E_{i,\max} = E_{eg}/2$ and $E_{i,\min} = E_{eg}/2 - E_0$, as seen in Eqs.(9) and (10) with $\boldsymbol{p}_{eg} = 0$. The trigger photon energy E_0 must be close to $E_{eg}/2$ to probe the neutrino thresholds in RENP, which is give by $E_{eg}/2 - (m_i + m_j)^2/2E_{eg}$ for $\boldsymbol{p}_{eg} = 0$, where $m_{i,j}$ denote the neutrino masses. Hence, $0 \lesssim E_i \leq E_{eg}/2$, as exemplified by the solid magenta line in Fig. 4. The upper half of this range must be in the forbidden band near the light line, defined by $E = \beta$, and this is not the case for the realistic Bragg fiber as illustrated in Fig. 4. The McQ3 suppression is $O(10^{-2})$ even for large N_p. The detailed analysis of this difficulty is given in Ref. [13].
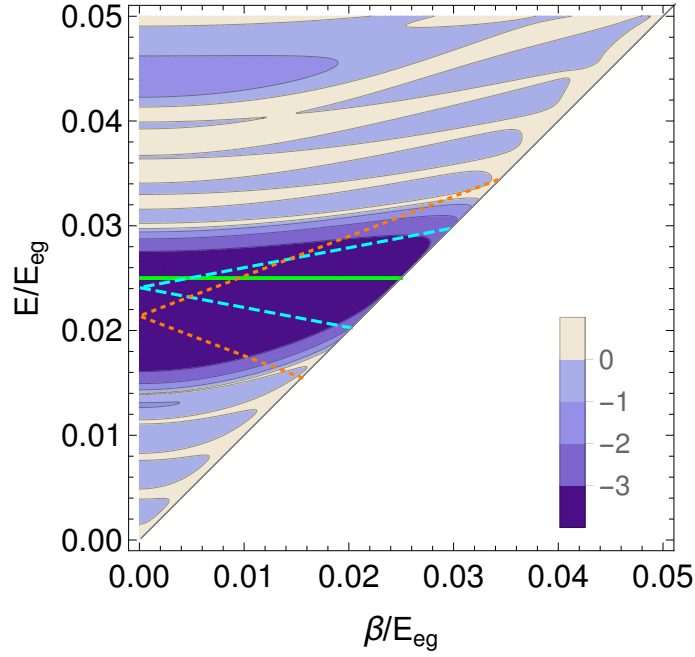
Figure 5: Purcell factor of the Bragg fiber designed to suppress the McQ3 with the BTL method. The index pair is the same as Fig. 4. The solid green horizontal line represents the McQ3 physical line in the BTL mode. The cyan dashed and orange dotted lines express the McQ3 physical lines of off-BTL cases.

5.2 Boost-Trigger lock

There are two possible directions to solve the above problem: To make the band gap wider and/or to make the photon spectrum narrower. The former is investigated in our previous work [13]. We can take the latter in the case of the boosted McQ3.

Suppose that the trigger momentum is locked to that of the boost,[1]

$$\boldsymbol{p}_{eg} = \boldsymbol{p}_0 \,, \tag{17}$$

so that $\boldsymbol{q} = 0$, that is, the center of mass of the photon pair $\gamma_1 \gamma_2$ is at rest in the laboratory frame. Then, we find

$$E_{i,\max} = E_{i,\min} = \frac{q^0}{2} = \frac{1}{2}(E_{eg} - E_0) =: E_{\mathrm{BTL}} \,, \tag{18}$$

namely, the spectrum of the emitted photons is monochromatic for a given trigger energy, $E_1 = E_2 = E_{\mathrm{BTL}}$. The propagation constants of the emitted photons are

$$\beta_i = E_{\mathrm{BTL}} |\cos \theta_i| \,, \ i = 1, 2. \tag{19}$$

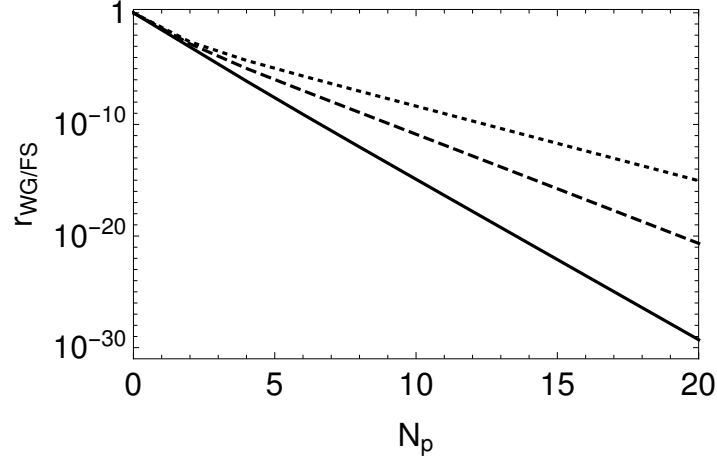[1]This may be achieved using the difference of two excitation lasers as the trigger.

Figure 6: McQ3 suppression factors in the Bragg fiber as functions of the number of layer pairs N_p. The other fiber parameters are the same as Fig. 5. The trigger energy is also the same as Fig. 5, $E_0 = 0.95E_{eg}$. Solid: the exact BTL case, $|\boldsymbol{p}_{eg}| = E_0$. Dashed (Dotted): the off-BTL case of $|\boldsymbol{p}_{eg}| = 0.990(0.988)E_0$.

The physical line on which the McQ3 events lie in the β–E plane is the straight section defined by $0 < \beta < E_{\mathrm{BTL}}$ and $E = E_{\mathrm{BTL}}$.

In Fig. 5, we illustrate the BTL physical line with $|\boldsymbol{p}_{eg}| = 0.95E_{eg}$, which is favored to enhance the signal sensitivity in the RENP of ytterbium target [9], as well as the Purcell factor of the Bragg fiber appropriate to suppress the McQ3 background with the BTL method. The parameters of the Bragg fiber are the same as Fig. 4 except $r_c/(a_1 + a_2) = 1$ and $E_{eg}(a_1 + a_2) = 10$. The BTL condition $|\boldsymbol{p}_{eg}| = E_0$ leads to the monochromatic photons of $E_{\mathrm{BTL}} = 0.05E_{eg}/2$. We observe that the both the emitted McQ3 photons are always in the forbidden band. As mentioned above, the lattice spacing $a_1 + a_2$ in Fig. 5is chosen as $E_{eg}(a_1 + a_2) = 10$ and much larger than that in Fig. 4. This is because of the lower energy scale of the emitted photons in the boosted McQ3 than the McQ3 without boost.

We also show two physical lines that deviate from the BTL condition for comparison. The case of $|\boldsymbol{p}_{eg}| = 0.99(0.98)E_0$ is expressed by the cyan dashed (orange dotted) line. We observe that the photon spectra extend toward the outside of the bad gap in these cases. We note, however, that the boost-trigger lock would not necessarily be exact. A tiny deviation of $\boldsymbol{q} = \boldsymbol{p}_{eg} - \boldsymbol{p}_0$ from 0 only leads to the energy width $E_{i,\max} - E_{i,\min} = |\boldsymbol{q}|$ as seen in Eqs. (9) and (10). The band gap that can accommodate this tiny energy width is possible with a reasonable index contrast.

5.3 Suppression of the BTL McQ3 in the Bragg fiber

The suppression factor of McQ3 in the Bragg fiber is given by Eq. (16) with the Purcell factor of the Bragg fiber. The solid line in Fig. 6 shows the McQ3 suppression factor in Eq. (16) in the BTL mode with $E_0 = 0.95E_{eg}$ as a function of the number of layer pairs
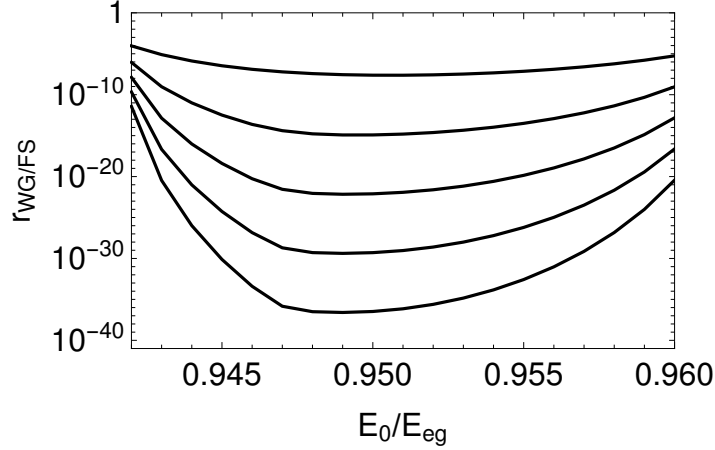
Figure 7: McQ3 suppression factors in the Bragg fiber with the BTL mode as functions of trigger energy for $N_p = 5, 10, 15, 20, 25$ (from top to bottom). The other fiber parameters are the same as in Fig. 5.

N_p. The other fiber parameters are the same as in Fig. 5. We observe the exponential behavior as inferred from the analytic argument in Ref. [13]. A suppression 10^{-23} or better is obtained for $N_p \gtrsim 16$.

In Fig. 6, we also present the McQ3 suppression factors in two cases of off-BTL, $|\boldsymbol{p}_{eg}| = 0.990(0.988)E_0$ in the dashed (dotted) line. In the present setup, the 1% deviation from the BTL limit is acceptable, but the further deviation easily leads to the failure of suppression.

In Fig. 7, the McQ3 suppression factors in the Bragg fiber with the BTL mode as functions of trigger energy for $N_p = 5, 10, 15, 20, 25$. The other fiber parameters are the same as in Fig. 5. We observe e.g. that the suppression is sufficient in the trigger range of $0.945E_{eg} < E_0 < 0.955E_{eg}$ for $N_p = 20$. For the Yb case ($E_{eg} = 2.14349$ eV) examined in Ref. [9], this means that we can scan the trigger range between 2.0256 eV and 2.0470 eV with suppressed McQ3 backgrounds. It is possible to modify this range by changing the overall scale (lattice spacing, $a_1 + a_2$) of the Bragg fiber. The width of this range is ~ 20 meV and practically independent of this scaling since we are interested in the narrow region near the endpoint ($\sim E_{eg}$, see below).

5.4 RENP spectrum in the BTL mode

As described above, the three momentum of the $\gamma_1\gamma_2$ system vanishes in the BTL mode, namely $\boldsymbol{q} = 0$. In other words, the $\gamma_1\gamma_2$ system is at rest in the laboratory frame. This also applies to the case of RENP, in which the $\nu_i\bar{\nu}_j$ system has $\boldsymbol{q} = 0$ and is at rest.
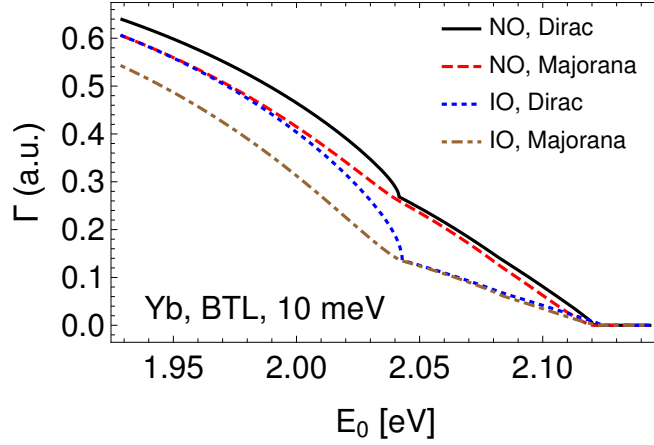
Figure 8: RENP spectrum in the BTL mode. The target is Yb and the light neutrino mass is 10 meV. The Majorana phases are taken to be 0. The same transition is employed as in Ref. [9]. The other neutrino parameters are the best-fit values taken from NuFIT 2018 [17].

Then the RENP spectral rate is simplified as

$$\Gamma^{\nu\bar{\nu}}_{\mathrm{BTL}}(E_0) = \Gamma^{\nu\bar{\nu}}_0 \sum_{i,j} \frac{\beta_{ji} q^2}{6(E_{pg} - E_0)^2} \frac{E_0}{E_{eg}} \left[|c^A_{ji}|^2 \left\{ 2 - \frac{m^2_j + m^2_i}{q^2} - \frac{(m^2_j - m^2_i)^2}{q^4} \right\} \right. \tag{20}$$

$$\left. - 6\delta_M \mathrm{Re}(C^{A2}_{ji}) \frac{m_j m_i}{q^2} \right], \tag{21}$$

where $c^A_{ji} = U^*_{ej} U_{ei} - \delta_{ji}/2$ with U being the PMNS matrix [16], q^2 is the invariant mass of the neutrino pair with q^μ given by Eq. (6), $\delta_M = 0(1)$ for Dirac (Majorana) neutrinos, and

$$\beta_{ji} := 1 - 2\frac{m^2_j + m^2_i}{q^2} + \frac{(m^2_j - m^2_i)^2}{q^4} . \tag{22}$$

The overall rate $\Gamma^{\nu\bar{\nu}}_0$ is given in Ref. [9].

We stress that the difference between Dirac and Majorana neutrinos and the dependence on the neutrino masses $m_{i,j}$ remain in the BTL mode. Namely, the neutrino mass spectroscopy including the Dirac-Majorana discrimination is possible in the BTL mode of RENP. In Fig. 8, we illustrate the RENP spectrum in the BTL mode for the case of Yb target ($E_{eg} = 2.14349$ eV) and the lightest neutrino mass of 10 meV. See Ref. [9] for details of the employed transition. The kink structure at thresholds and the difference between Dirac and Majorana are apparent.

The threshold of the trigger photon energy to produce a $\nu_i \bar{\nu}_j$ pair is given by $E_{eg} - (m_i + m_j)$ under the BTL condition. Using the 2018 results of NuFIT [17] and Planck [18] collaborations, we find that the upper bound of the lightest neutrino mass is 30.2 meV for

the normal ordering (NO) and 16.2 meV for the inverted ordering (IO). The mass range of the heaviest neutrino is [49.9, 58.4]([49.6, 52.2]) meV for NO(IO). It is possible to cover these mass ranges in the neutrino mass spectroscopy with a few fibers of different lattice spacings, since each Bragg fiber of fixed lattice spacing covers the mass range about 20 meV near the endpoint E_{eg} corresponding to the massless neutrinos as explained above.

6 Conclusion

We have studied the QED background process McQ3 against the atomic neutrino process RENP in the presence of the initial spatial phase. The macrocoherence amplifies RENP, but at the same time amplifying QED backgrounds.

To suppress the McQ3 process, we consider the experimental scheme that makes use of the hollow-core photonic crystal fiber. The photonic band gap of the crystal prohibits the photon emission in principle. The width of the band gap must be wide enough so that the relevant energy range of the emitted photons in McQ3 is covered.

We have found that the energy spectrum of McQ3 can be controlled by making the initial spatial phase factor $\boldsymbol{p}_{eg}$ locked to the momentum of the trigger photon (boost-trigger lock, BTL). The four-momentum conservation dictated by the macrocoherence implies that the center of mass of the emitted photon pair in McQ3 is at rest in the BTL mode, so that the photon spectrum is monochromatic. We have shown that the sufficient suppression of McQ3 in the Bragg fiber is possible using the BTL method.

The RENP spectrum in the BTL mode has also been examined. It is found that the dependence on the neutrino masses and the difference between Dirac and Majorana neutrinos remain sizable in the RENP spectrum in the BTL mode. We have found that a set of a few fibers of different lattice spacings is sufficient to scan the region sensitive to neutrino masses.

To summarize, the McQ3 QED background problem in the atomic neutrino process RENP can be solved in principle using a photonic crystal fiber. The BTL method that makes use of the initial spatial phase works with the Bragg fiber of the realistic combination of refractive indices.

Acknowledgments

References

[1] D. N. Dinh, S. T. Petcov, N. Sasao, M. Tanaka, and M. Yoshimura, "Observables in Neutrino Mass Spectroscopy Using Atoms," *Phys. Lett.* **B719** (2013) 154–163, `arXiv:1209.4808 [hep-ph]`.

[2] A. Fukumi *et al.*, "Neutrino Spectroscopy with Atoms and Molecules," *PTEP* **2012** (2012) 04D002, `arXiv:1211.4904 [hep-ph]`.

[3] M. Yoshimura, C. Ohae, A. Fukumi, K. Nakajima, I. Nakano, H. Nanjo, and N. Sasao, "Macro-coherent two photon and radiative neutrino pair emission," `arXiv:0805.1970 [hep-ph]`.

[4] M. Yoshimura, N. Sasao, and M. Tanaka, "Dynamics of paired superradiance," *Phys. Rev.* **A86** (2012) 013812, `arXiv:1203.5394 [quant-ph]`.

[5] Y. Miyamoto, H. Hara, S. Kuma, T. Masuda, I. Nakano, C. Ohae, N. Sasao, M. Tanaka, S. Uetake, A. Yoshimi, K. Yoshimura, and M. Yoshimura, "Observation of coherent two-photon emission from the first vibrationally excited state of hydrogen molecules," *PTEP* **2014** no. 11, (2014) 113C01, `arXiv:1406.2198 [physics.atom-ph]`.

[6] Y. Miyamoto, H. Hara, T. Masuda, N. Sasao, M. Tanaka, S. Uetake, A. Yoshimi, K. Yoshimura, and M. Yoshimura, "Externally triggered coherent two-photon emission from hydrogen molecules," *PTEP* **2015** no. 8, (2015) 081C01, `arXiv:1505.07663 [physics.atom-ph]`.

[7] Y. Miyamoto, H. Hara, T. Masuda, N. Sasao, S. Uetake, A. Yoshimi, K. Yoshimura, and M. Yoshimura, "Vibrational two-photon emission from coherently excited solid parahydrogen," *The Journal of Physical Chemistry A* **121** no. 20, (2017) 3943–3951, `https://doi.org/10.1021/acs.jpca.7b02011`. `https://doi.org/10.1021/acs.jpca.7b02011`. PMID: 28459577.

[8] T. Hiraki, H. Hara, Y. Miyamoto, K. Imamura, T. Masuda, N. Sasao, S. Uetake, A. Yoshimi, K. Yoshimura, and M. Yoshimura, "Coherent two-photon emission from hydrogen molecules excited by counter-propagating laser pulses," *J. Phys.* **B52** no. 4, (2019) 045401, `arXiv:1806.04005 [physics.atom-ph]`.

[9] M. Tanaka, K. Tsumura, N. Sasao, S. Uetake, and M. Yoshimura, "Effects of initial spatial phase in radiative neutrino pair emission," *Phys. Rev.* **D96** no. 11, (2017) 113005, `arXiv:1710.07136 [hep-ph]`.

[10] M. Yoshimura, N. Sasao, and M. Tanaka, "Radiative emission of neutrino pair free of quantum electrodynamic backgrounds," *PTEP* **2015** no. 5, (2015) 053B06, `arXiv:1501.05713 [hep-ph]`.

[11] P. Yeh, A. Yariv, and E. Marom, "Theory of Bragg fiber," *J. Opt. Soc. Am.* **68** (1978) 1196.

[12] J. D. Joannopoulos, S. G. Johnson, J. N. Winn, and R. D. Meade, *Photonic Crystals.* Princeton University Press, second ed., 2008.

[13] M. Tanaka, K. Tsumura, N. Sasao, and M. Yoshimura, "Toward background-free RENP using a photonic crystal waveguide," *PTEP* **2017** no. 4, (2017) 043B03, arXiv:1612.02423 [physics.optics].

[14] Y. Fink, D. J. Ripin, S. Fan, C. Chen, J. D. Joannepoulos, and E. L. Thomas, "Guiding optical light in air using an all-dielectric structure," *J. Lightwave Technol.* **17** no. 11, (Nov, 1999) 2039–2041.

[15] E. M. Purcell, "Spontaneous emission probabilities at radio frequencies," *Phys. Rev.* **69** (1946) 681.

[16] **Particle Data Group** Collaboration, M. Tanabashi *et al.*, "Review of particle physics," *Phys. Rev. D* **98** (Aug, 2018) 030001. https://link.aps.org/doi/10.1103/PhysRevD.98.030001.

[17] I. Esteban, M. C. Gonzalez-Garcia, M. Maltoni, I. Martinez-Soler, and T. Schwetz, "Updated fit to three neutrino mixing: exploring the accelerator-reactor complementarity," *Journal of High Energy Physics* **2017** no. 1, (Jan, 2017) 87, arXiv:1611.01514.

[18] **Planck** Collaboration, N. Aghanim *et al.*, "Planck 2018 results. VI. Cosmological parameters," arXiv:1807.06209 [astro-ph.CO].